Monte Carlo Study and Experimental Measurements of Breast Tumor Detectability with the YAP-PEM prototype

Alberto Del Guerra [1], Nicola Belcari [1],Walter Bencivelli [2], Alfonso Motta [1], Sergio Righi [1], Angela Vaiano [1], Giovanni Di Domenico [3], Elena Moretti [3], Nicola Sabba [3], Guido Zavattini [3], Renato Campanini [4], Nico Lanconelli [4], Alessandro Riccardi [4], M. Nerina Cinti [5], Roberto Pani [5], Rosanna Pellegrini [5]

***Abstract*-- A prototype for positron emission mammography is under development within a collaboration of the Italian Universities of Pisa, Ferrara, Bologna and Roma. The device is composed of two stationary detection heads, each with an active area of 6 cm × 6 cm, made of 30×30 YAP:Ce finger crystals of 2 mm × 2 mm × 30 mm. The EGSnrc Monte Carlo code has been used to perform a complete simulation of this camera. We have used a fast three-dimensional iterative algorithm (30 s per iteration on a PC-Pentium III 800 MHz processor) for image reconstruction. The performed study indicates that tumors of 5 mm diameter, i.e., 0.065 cm^3 volume, with 37 kBq/cm^3 (1 μCi/cm^3) specific activity embedded in a breast active phantom, are detectable in 10 minutes for a 10:1 tumor/background ratio with an 8.7 Signal-to-Noise Ratio value. Experimental measurements with the small animal tomograph YAP-PET have validated the Monte Carlo predictions.**

I. Introduction

X-ray mammography is a fundamental technique for breast cancer screening. However, radiological examinations are not always diagnostic, and for these cases a biopsy is usually done. Alternatively, a less traumatic and noninvasive PET examination could be performed. Whole body PET cameras are often used, but dedicated devices with high sensitivity and high spatial resolution are needed. In this respect, many groups are developing dedicated devices for Positron Emission Mammography (PEM) [1]-[8].

II. The YAP-PEM prototype

We are developing a PEM prototype based on Yttrium Aluminum Perovskite scintillators doped with Cerium (YAP:Ce) and Position Sensitive Photomultiplier Tubes (PSPMT's). The device should be able to detect breast lesions, with dimensions of 5 mm in diameter, and with a specific activity ratio of 10:1 between the cancer and breast tissue. The implemented detector technology derives from our previous experience in small animal imaging scanners [9], [10]. The camera consists of two opposite heads, whose dimensions are (6 cm × 6 cm) area × 3 cm thickness. Each head is composed of 30 × 30 YAP:Ce finger crystals of 2 mm × 2 mm × 30 mm (Fig.1). It has been shown that breast compression increases the lesion detectability, especially for cancers lying near the thorax [11]. Hence, each matrix will be equipped with a compressor of 1 cm thick Perspex. A 50 μm tungsten sheet will be placed between the crystal matrix and the compressor, so as to further shield the background of low energy photons. The distance between the two heads determines the Field of View (FOV) axial dimension and can range from 5 cm to 10 cm, depending on the compression status.

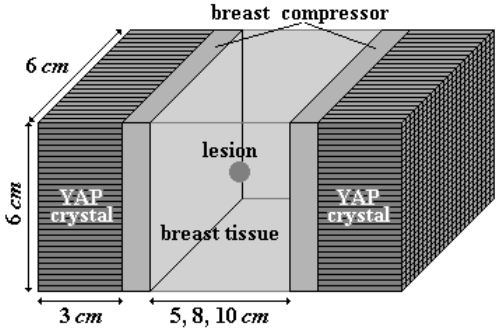

Fig. 1. YAP-PEM prototype design: two 6 cm × 6 cm × 3 cm matrices of YAP:Ce crystals with PSPMT's readout (not shown in the figure). 900 finger crystals of 2 mm × 2 mm × 30 mm compose each matrix. A breast compressor of 1 cm Perspex is mounted in front of each detection head. The distance between the two heads ranges between 5 and 10 cm. The lesion/tissue specific activity ratio is 10:1

III. Monte Carlo simulation

The Monte Carlo code used is EGSnrc [12]. The simulated phantoms are spherical tumors of variable size positioned

1-Dept. of Physics, University of Pisa and INFN Branch of Pisa, Via F. Buonarroti 2, 56127, Pisa, Italy
2-Dept. of Internal Medicine, University of Pisa, Via Roma 67, 56126, Pisa, Italy
3-Dept. of Physics, University of Ferrara and INFN Branch of Ferrara, Via Paradiso 2, 44100, Ferrara, Italy
4-Dept. of Physics, University of Bologna and INFN Branch of Bologna, Viale B. Pichat 6/2, 40127, Bologna, Italy
5-Dept. of Experimental Medicine, University of Roma "La Sapienza", P.le A. Moro 5, 00185, Roma, Italy

0-7803-7636-6/03/$17.00 ©2003 IEEE.

inside an active region of breast tissue. The latter is simulated as a uniform slab, whose chemical and physical characteristics are those given by ICRU-44 [13]. Breast compression can be moderate, middle and strong, in the simulation for a compressor distance of 10, 8, and 5 cm, respectively. Scattering from the outside of the FOV is not considered, i.e., the thorax is not simulated. A tumor specific activity of 37 kBq/cm^3 (1 μCi/cm^3) and a background (active breast tissue) specific activity of 3.7 kBq/cm^3 (0.1 μCi/cm^3) are always assumed, thus giving a 10:1 tumor/background (T/B) ratio.

The code simulates the positron emission with its continuous spectrum, the positron slowing down and annihilation, with appropriate non co-linearity sampling, and the interaction of the photons in breast tissue, in the Perspex compressor and tungsten sheet, and within the YAP scintillator. We transport photons and electrons within the phantom with a common low energy cut-off of 50 keV. We follow the photon in the YAP crystal down to the cut-off energy of 10 keV. We do not perform electron transport within the detector. Each energy deposition (E) is folded with the appropriate resolution, scaled as $(E)^{-1/2}$ from the energy resolution of 25% at 511 keV, which we have previously measured with the YAP-PET tomograph [9]. For multiple energy depositions, the photon interaction coordinates are determined by energy weighting. No simulation of the PSPMT readout is performed.

We studied the detectability of the tumor according to its size and position in the FOV, and the effects of breast compression. The developed simulation has been validated by comparison with experimental results.

IV. Three-dimensional iterative reconstruction

Since the stationary acquisition with planar detectors implies incomplete angular sampling, backprojection methods reconstruct images in the planes parallel to the detector surface with heavy blurring, either with or without applying single slice rebinning [14]. Therefore, there is the need to use three-dimensional (3D) iterative techniques to produce a pseudo-tomographic imaging [14]-[17]. We adapted the EM algorithm developed for the YAP-PET tomograph [18], [19] to our PEM prototype, so as to use all the possible *lines of response* (LOR's) in the FOV. The drawback of EM algorithm is the long computation time. Various methods have been introduced in the literature to reduce the computational time and increase the spatial resolution [20]-[27]. We developed a deconvolution technique that takes advantage of both sparse properties and symmetries of our detector, and considers both the tube-voxel intersection and solid angle calculation. By using this approach we reduce the storage space of the probability matrix to few megabytes. The probability computation requires less than 10 s with a PC-800 MHz processor, while a reconstruction time of 30 s per iteration is obtained. The reconstruction gives 3D volume images. For the almost planar nature of the data, final image is already reached at the first iteration. This image is then smoothed so as to reduce increase of noise at the image edges. At this time, attenuation and scattering models are not considered in our reconstruction.

V. Results of Monte Carlo simulations

We measured the Signal to Noise Ratio (SNR) in the reconstructed image as a function of the tumor size and its position, of the statistics of the data, and of the compression status. All performed studies simulate a 10 minutes acquisition time. Since ^{18}F-FDG will be used in the clinical applications, the source is always the ^{18}F radioisotope, with its continuous spectrum.

The first study analyzes the detectability as a function of the tumor size, by varying the volume of spherical sources from 1.0 cm^3, corresponding to a diameter of 12.4 mm, down to 0.065 cm^3, i.e., a diameter of 5.0 mm. The tumor is embedded in active breast tissue at the center of the FOV. We considered a distance between the detector heads of 5 cm (strong compression). An energy threshold of 50 keV in the detector is used. The Signal to Noise Ratio (SNR) is measured on the reconstructed images (1 mm slices) by using the definition

$$SNR = \frac{T - B}{\sigma_B},$$

where T is the average signal inside the area covered by the tumor, B is the average background in an equal area of tissue, and σ_B is the standard deviation of B. The obtained SNR values are reported in Fig. 2: all values are greater than 5, the conventional limit of visibility in analog radiology.

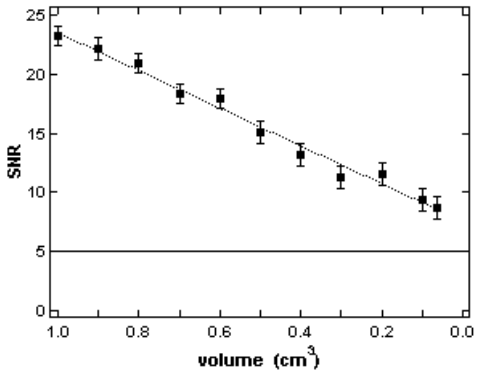

Fig. 2. SNR values obtained from reconstructed images of simulated tumors, whose sizes vary from a 1.0 cm^3 volume down to 0.065 cm^3 (corresponding to 5.0 mm tumor diameter). The SNR equal to 5 line, i.e., the conventional limit of visibility in analog radiology, is also reported.

The obtained images of the tumors and their profiles are shown in Fig. 3 and Fig. 4, respectively. Lesions are clearly visible in all cases. Images are not filtered, and are in 256 gray-tones, where 0 corresponds to the minimal value in tissue and 255 to the maximum value for each image. We show the central plane 1 mm slice, where the tumor lies.

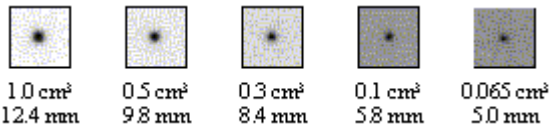

Fig. 3. Reconstructed images of different volume tumors, from a spherical source of 1.0 cm^3 down to 0.065 cm^3. No filtering is applied. Images are in 256 gray-tone, from the background minimum value to the maximum: each image is normalized to its own maximum. The tumor lies at FOV center in active breast tissue, with a specific activity ratio 10:1 between cancer (37 kBq/cm^3, i.e., 1.0 $\mu Ci/cm^3$) and tissue (3.7 kBq/cm^3, i.e., 0.1 $\mu Ci/cm^3$). The detector head distance is 5 cm. We show the central 1 mm slice image, where the tumor lies.

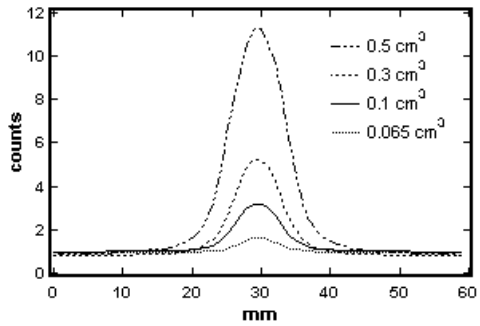

Fig. 4. Profiles of different tumors, whose volume sizes varies from 0.5 cm^3 down to 0.065 cm^3. Profiles are shown for the central slice non-normalized images. The images have been previously smoothed.

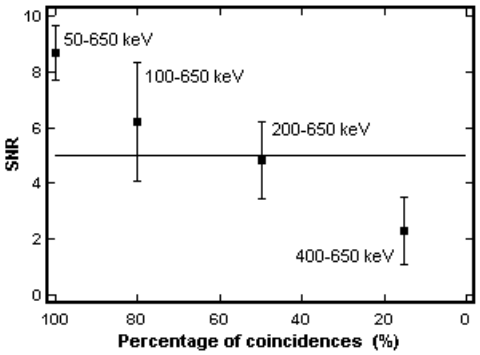

Fig. 5. SNR values versus percentage of accepted coincidence for various energy windows, for the 5.0 mm diameter tumor, i.e., 0.065 cm^3, and strong breast compression (5 cm). The same energy window is applied to both detectors. The line of the conventional limit of visibility in analog radiology (SNR=5) is also shown.

Fig. 6. Tumor images for various energy windows, for the 5 mm diameter tumor (0.065 cm^3), and strong breast compression. Each image is 256 gray-tone, from the minimum value of background to the maximum value; each image is normalized to its own maximum. The central 1 mm slice image is shown, where the tumor lies.

The SNR values depend on the detection energy window. This dependence is shown in Fig. 5, for a tumor of 5 mm diameter (0.065 cm^3), in strong compression status. We consider a lower threshold of 50, 100 and 200, and 400 keV, and an upper of 650 keV. The corresponding images are shown in Fig. 6.

The simulation of the effect of breast compression is made by varying the distances between the detectors: 5, 8 and 10 cm for strong, middle and moderate compression respectively. We consider the breast as an incompressible fluid. Fig. 7 shows the results for the 5.0 mm diameter tumor (0.065 cm^3). The measured SNR values are 8.7±1.0, 3.6±1.4 and 2.2±1.1 with detector distance of 5, 8 and 10 cm, respectively, for the 50-650 keV energy window.

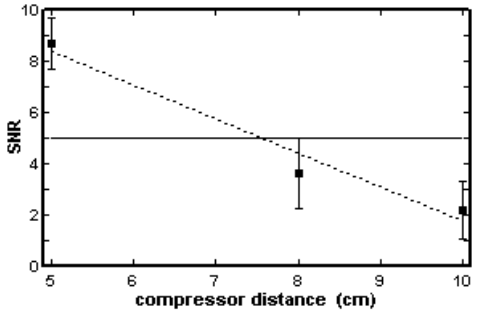

Fig. 7. SNR dependence on compression status. Three compressor distances of 5, 8 and 10 cm are considered, i.e., strong, middle and moderate compression. The tumor has a diameter of 5 mm (0.065 cm^3). A 50-650 keV energy window has been used. The line of the conventional limit of visibility in analog radiology (SNR=5) is also shown.

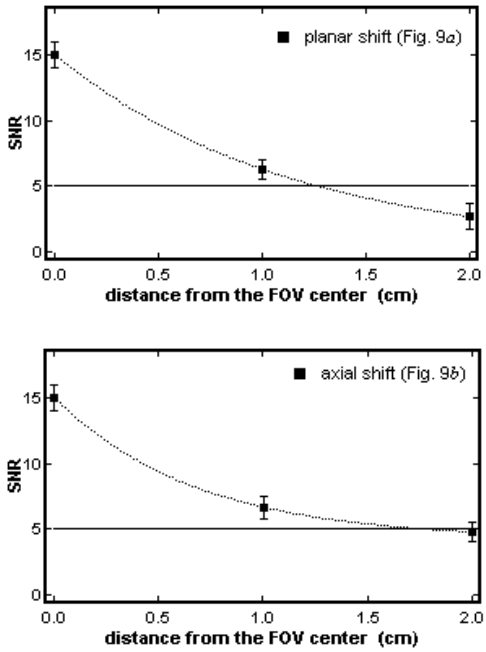

Fig. 8. Tumor detectability as a function of distance from the center of the FOV: along the axis parallel to the detector plane (*a*); along the orthogonal axis (*b*). The tumor has a volume of 0.5 cm^3, i.e., a diameter of 9.8 mm. An energy window of 50-650 keV is applied, for a strong compression condition.

The dependence of the tumor detectability on its position within the FOV is shown in Fig. 8. The 0.5 cm^3 tumor (9.8 mm diameter) is positioned at the center of the FOV and then

translated by 1 cm steps on the central plane along the axis parallel to both detector faces (Fig. 8*a*) and along the orthogonal axis (Fig. 8*b*). The energy window is 50-650 keV, for a strong compression condition.

VI. Experimental Measurements

An experiment has been performed with the small animal YAP-PET tomograph [9], [10] to image in planar geometry a phantom that simulates breast lesions. The experiment was performed with only one pair of opposite detectors, 15 cm far away. Each head has a size of 4 cm × 4 cm × 3 cm, with 20 × 20 YAP:Ce finger crystals of 2 mm × 2 mm × 30 mm. The simulated breast is a specially designed solid phantom: a ^{68}Ge planar source of 925 kBq (25 μCi), which simulates a cylinder of 10.8 cm diameter and 6 cm height. Three size tumors are simulated by cylinders with diameters of 0.3, 0.5 and 1.0 cm, with activities of 370 Bq (10 nCi), 1.6 kBq (44 nCi) and 12.9 kBq (350 nCi), respectively. Each cylinder height is equal to its diameter. Stationary acquisitions are performed for combinations of cylinder sources (tumors) with the planar source (breast tissue). Specific activity T/B ratio is about 10:1 for all acquisitions. The reconstructed images are presented in Fig. 9 (*top row*). The ^{68}Ge planar source introduces additional structured background due to its granularity (Fig. 9, *middle row*). We subtracted this additional background from the reconstructed images of the tumors (Fig. 9, *bottom row*). The halo surrounding the tumors is probably due to high kinetic energy ^{68}Ge positrons, which annihilate in the planar source far from the cylinders.

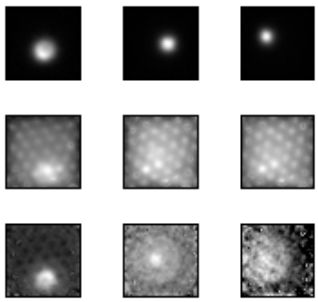

Fig. 9. Reconstructed images of dedicated ^{68}Ge solid breast phantoms, acquired with two opposite heads of the YAP-PET tomograph. Tumors (*top row*) are cylindrical sources of 1.0 cm (*a*), 0.5 cm (*b*) and 0.3 cm (*c*) diameter. Tumors in breast tissue are simulated by putting the high activity cylinders on the planar source (*middle row*). The *bottom row* shows the images obtained after the subtraction of the structured background due to the granularity of the planar source. Images are scaled in 256 gray-tones with respect to their own maximum value. No filtering is applied. We show the slice where the tumor lies.

A. Comparison of Experimental Results with Monte Carlo Predictions

The experimental acquisitions have been reproduced via Monte Carlo. The only differences are that the simulated positron source is ^{18}F with its continuous spectrum (not ^{68}Ge), and the simulated tumor is embedded in breast tissue. The images of these simulations are shown in Fig. 10.

Numerical SNR values for experimental and Monte Carlo results are reported in Table I.

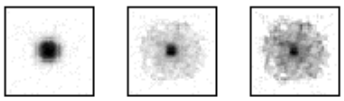

Fig. 10. Iterative images of Monte Carlo simulations reproducing the experimental YAP-PET acquisitions of dedicate breast phantoms, for tumors of 1.0 cm (*a*), 0.5 cm (*b*) and 0.3 cm (*c*), embedded in simulated breast background of 6 cm. The images are scaled in 256 gray-tone from the medium value of background to its own maximum. No filtering is applied. We show the 1 mm slice where the tumor lies.

Table I. Comparison between SNR values of a YAP-PET experimental acquisitions of dedicated breast phantoms and corresponding Monte Carlo predictions.

cylindrical source		SNR	
diameter (*cm*)	activity (*nCi*)	YAP-PET measurements	Monte Carlo predictions
1.0	350	31.2 ± 3.9	34.7 ± 5.1
0.5	44	8.6 ± 1.2	11.9 ± 3.2
0.3	10	9.4 ± 1.4	9.0 ± 1.5

VII. Discussion and Conclusion

The Monte Carlo simulation shows that the proposed PEM prototype is able to detect all size tumors down to 0.065 cm^3 (5.0 mm diameter), when positioned at the center of the FOV, with a T/B specific activity ratio of 10:1, i.e., Fig. 2, Fig. 3 and Fig. 4. The measured SNR values seem to linearly depend on tumor volume size (Fig. 2).

The SNR values are strongly dependent on the acquired statistics. In simulated cases, the reduction of the width of the energy window of the detectors also reduces the measured SNR (Fig. 5). In our stationary prototype the use of the lowest energy threshold enhances the detectability of the tumor. We expect that this could change when the scatter from thorax is considered.

This simulation confirms the important role of breast compression (Fig. 7), especially to detect the smallest tumors (a volume smaller than 0.1 cm^3). A strong compression (i.e., 5 cm thick breast) allows to see the 0.065 cm^3 tumor (5.0 mm diameter), with a good SNR value (SNR = 8.7±1.0).

The background from breast tissue activity compromises the detectability of tumors lying far from the FOV center. A tumor of 0.5 cm^3 volume (9.8 mm diameter) is always detectable within a 1.0 cm distance from the FOV center; but its measured SNR decreases under the value of 5 already at a distance of 2 cm from the center (Fig. 8). This would indicate that with a T/B ratio of 10:1 the 6 cm × 6 cm active area assures high

detectability in the central 4 cm × 4 cm of the FOV; outside this area the tumor detectability has a SNR less than 5.

The developed Monte Carlo simulator has been fully validated by the comparison with experimental data obtained with the YAP-PET tomograph (i.e., see Table I).

VIII. REFERENCES

[1] C.J. Thompson, K. Murthy, Y. Picard, I. N. Weinberg, and R. Mako, "Positron Emission Mammography (PEM): A promising technique for detecting breast cancer," IEEE Trans. Nucl. Sci., vol. 42, no. 2, pp. 1012-1017, Aug. 1995

[2] I. Weinberg, S. Majewski, A. Weisenberger, A. Markowitz, L. Aloj, L. Majewski, D. Danforth, J. Mulshine, K. Cowan, J. Ujewski, C. Chow, E. Jones, V. Chang, W. Berg, and J. Frank, "Preliminary results for positron emission mammography: real time functional breast imaging in a conventional mammography gauntry," Eur. J. Nucl. Med., vol. 23, no. 7, pp. 804-806, Jul. 1996

[3] K. Murthy, M. Aznar, C. J. Thompson, A. Loufti, R. Lisbona, and J. H. Gagnon, "Results of preliminary clinical trials of the positron emission mammography system PEM-1: A dedicated breast imaging system producing glucose metabolic images using FDG," J. Nucl. Med., vol. 41, pp. 1851-1858, 2000

[4] K. Murthy, M. Aznar, A. M. Bergman, et al., "Positron emission mammographic instrument: initial results," Radiology, vol. 215, pp. 280-285, 2000

[5] R. Freifelder, and J. S. Karp, "A dedicated PET scanner for breast cancer," Phys. Med. Biol., vol. 42, pp. 2463-2480, 1997

[6] K. Murthy, D. Jolly, M. Aznar, et al., "Qualification in positron emission mammography (PEM) with planar detectors: contrast resolution measurements using a custom breast phantom and novel spherical hot-spots," IEEE Trans. Nucl. Sci., vol. 46, pp. 2192-2196, 1999

[7] J. L. Robar, C. J. Thompson, K. Murthy, R. Clancy, and A. M. Bergman, "Construction and calibration of detectors for high resolution metabolic breast cancer imaging," Nucl. Inst. Meth. Phys. Res., vol. A392, pp. 402-406, 1997

[8] A. M. Bergman, C. J. Thompson, K. Murthy, et. al., "Technique to obtain positron emission mammography images in registration with X-ray mammograms," Med. Phys., vol. 25, pp. 2119-2129, 1998

[9] A. Del Guerra, C. Damiani, G. Di Domenico, M. Giganti, R. Marchesini, A. Motta, A. Piffanelli, N. Sabba, L. Sartori, and G. Zavattini, "An integrated PET-SPECT small animal imager: preliminary results," IEEE Trans. Nucl. Sci., vol. 47, pp. 1537-40, 2000

[10] G. Di Domenico, A. Motta, G. Zavattini, A. Del Guerra, C. Damiani, V. Bettinardi, and M. C. Gilardi, "Characterization of the Ferrara animal PET scanner," Nucl. Instr. And Meth., vol. A477, pp. 505-8, 2002

[11] R. Pani, A. Soluri, I. N. Weinberg, G. De Vincentis, R. Scafé, M. N. Cinti, L. Indovina, F. Scopinaro, V. David, F. Garibaldi, A. Del Guerra, and I. Khalkhali, "The role of breast compression in scintimmammography," Conference Records of the IEEE Nucl. Sci. Symposium and Medical Imaging Conference 2000, Lyon, France, 15-20 October 2000, ISBN-0-7803-6506-2 (CD-ROM), pp. 2696-2698, 2001

[12] I. Kawrakow and D. W. O. Rogers, "The EGSnrc code system: Monte Carlo Simulation of electron and photon transport," Technical Report PIRS-701, National Research of Canada, Ottawa, Canada, 2000

[13] ICRU, "Tissue Substitutes in Radiation Dosimetry and Measurement," Report 44 of the International Commission on Radiation Units and Measurements, Bethesda, MD, USA, 1989

[14] M. F. Smith, S. Majewski, A. G. Weisenberger, D. Kieper, J. D. Kalen, and P. P. Fatouros, "Aspect of 3-D imaging by classical tomography for dual detector PEM," Book of "3D-2001, The Sixth International Meeting on Fully Three-Dimensional Image Reconstruction in Radiology and Nuclear Medicine", , pp. 211-214, Pacific Grove, California, USA, October 30- November 2, 2001

[15] P. E. Kinahan, D. Brasse, M. Defrise, R. Clackdoyle, C. Comtat, C. Michel, and X. Liu, "Fully 3D iterative reconstruction of planogram data," Book of "3D-2001, The Sixth International Meeting on Fully Three-Dimensional Image Reconstruction in Radiology and Nuclear Medicine", pp. 21-24, Pacific Grove, California, U.S.A., October 30-November 2, 2001

[16] L. A. Shepp, and Y. Vardi, "Maximum likelihood reconstruction for emission tomography," IEEE Trans. Med. Imag., vol. 1, no. 2, pp. 113-122, 1982

[17] L. Parra, and H. H. Barrett, "List-mode likelihood: EM algorithm and image quality estimation demonstrated on 2-D PET," IEEE Trans. Med. Imag., v17, n.2, pp. 228-235, 1998

[18] A. Motta, "Fast algorithm for iterative image reconstruction with a small animal positron emission tomograph YAP-PET," (Ph.D. Thesis Abstract) Medical Physics, vol. 28, no. 6, pp. 1141, June 2001

[19] A. Motta, C. Damiani, A. Del Guerra, G. Di Domenico, and G. Zavattini, "Use of a fast EM algorithm for 3D image reconstruction with the YAP-PET tomograph", Comput. Med. Imag. Graph., vol. 26, no. 5, pp. 293-302, Aug. 2002

[20] P. Kinahan, C. Michel, and M. Defrise, "Fast iterative image reconstruction of 3D PET data," Conference Records of the IEEE Nuclear Science Symposium and Medical Imaging Conference (Anaheim, CA, 1996), Ed A. Del Guerra (Piscataway, NJ:IEEE) pp. 1918-1922, 1996

[21] M. L. Egger, C. Joseph, and C. Morel, "Incremental beamwise backprojection using geometrical symmetries for 3D PET reconstruction in a cylindrical scanner geometry," Phys. Med. Biol., vol. 43, pp. 3009-3024, 1998

[22] C. Chen, S. Lee, and Z. Cho, "Parallelization of the EM algorithm for 3D PET image reconstruction," IEEE Trans. Med. Imaging., vol. 110, pp. 513-522, 1991

[23] C. A. Johnson, Y. Yan, R. E. Carson, R. Martino, and M. E. Daube-Witherspoon, "A system for the 3D reconstruction of retracted-septa PET data using the EM algorithm," IEEE Trans. Nucl. Sci., *vol.* 42, pp. 1223-1227, 1995

[24] C. A. Johnson, J. Seidel, R. E. Carson, W. R. Gandler, A. Sofer, M. Green, and M. E. Daube-Witherspoon, "Evaluation of 3D reconstruction algorithms for a small animal PET camera," IEEE Trans. Nucl. Sci., vol. 44, pp. 1303-8, 1997

[25] J. M. Ollinger, and A. S. Goggin, "Maximum Likelihood reconstruction in fully 3D PET via the SAGE algorithm," Conference Records of the IEEE Nuclear Science Symposium and Medical Imaging Conference (Anaheim, CA, 1996), Ed A Del Guerra (Piscataway, NJ:IEEE), pp. 1594-8, 1996

[26] A. Terstegge, S. Weber, H. Herzog, H. W. Muller-Gartner, and H. Hailling, "High resolution and better quantification by tube of response modeling in 3D PET reconstruction," Conference Record of the IEEE Nuclear Science Symposium and Medical Imaging Conference (Anaheim, CA, 1996), Ed A Del Guerra (Piscataway, NJ:IEEE), pp. 1603-7, 1996

[27] J. Qi, R. M. Leahy, S. R. Cherry, A. Chatziioannou, and T. H. Farquhar, "High-resolution 3D Bayesian image reconstruction using the microPET small-animal scanner," Phys. Med. Biol., vol. 43, pp. 1001-1013, 1998